



Highly stretchable graphene/polydimethylsiloxane composite lattices with tailored structure for strain-tolerant EMI shielding performance

Zhenyu Wang^{a,b}, Wenzhen Yang^a, Rui Liu^a, Xingle Zhang^a, Hengyong Nie^c, Yu Liu^{a,b,d,*}

^a School of Mechanical Engineering, Jiangnan University, Wuxi, China

^b Jiangsu Key Laboratory of Advanced Food Manufacturing Equipment and Technology, Jiangnan University, Wuxi, China

^c Surface Science Western, Western University, London, Canada

^d School of Design, Jiangnan University, Wuxi, China

ARTICLE INFO

Keywords:

Graphene
Nano composites
Electromagnetic interference shielding (EMI)
3D printing
Stretchable composites

ABSTRACT

The fast-growing wearable and portable electronics bring imperative demand for high-performance stretchable electromagnetic interference (EMI) shielding materials to tackle the issue of electromagnetic (EM) wave pollution. In this work, highly stretchable and conductive graphene/polydimethylsiloxane lattices are fabricated through a facile 3D printing technique. Benefiting from the unique 3D interconnected and robust conductive network, the resultant composite lattices deliver excellent stretchability of 130%, tunable EMI shielding effectiveness (SE) as high as 45 dB, along with exceptional durability, showing over 90% retention of EMI SE even after 200 cycles of repeated stretching and releasing at strains up to 100%. In addition, the composite lattices exhibit outstanding shielding stability, because the deformation of lattice structure effectively shares the external strain, and the filaments perpendicular to the loading direction act as stabilizing layers preventing the steep resistance changes. The exceptional combination of mechanical properties and EMI shielding performance of the composite lattice provide a brand new perspective for next-generation flexible and stretchable electronics.

1. Introduction

The flourishing development of next-generation flexible electronic devices, including flexible displays, wearable human health monitoring systems, and foldable e-papers, have brought tremendous convenience and entertainment to people's daily life. However, the extensive use of these electronic devices would generate electromagnetic interference (EMI), which might cause malfunction of electronic system and have detrimental impacts on human health [1]. Thus, EMI is a significant issue in modern society and the development of EMI shielding materials has become an area of intense research. Traditional heavy metal-based EMI shielding materials cannot fulfill the requirement for flexible electronics, which suffers from high density, weak flexibility and poor anticorrosion [2]. From the point of view of wearable technology, proper candidates are expected to possess not only exceptional deformation capabilities, but also outstanding and stable EMI shielding effectiveness (SE) under complicated external loadings, such as stretching, bending, and twisting.

Polymer based composites filled with various conductive fillers are widely considered to be one of the most promising stretchable EMI

shielding materials [3]. Huge efforts have been made to rationally design and construct high-quality conductive network inside stretchable polymer matrixes using a variety of conductive fillers, including 0D conductive particles [4], 1D metal nanowires [5] and nanotubes [6], along with 2D graphene [7] and MXene [8]. Although significant progress in improving the EMI SE, stretchability, and durability of conductive polymer composites has been achieved, the instability of EMI shielding properties at large external deformations is still a critical issue. It has been well established that the EMI shielding performance of conductive polymer composites is strongly associated with their electrical conductivities, which is in turn related to the quality of the inner conductive networks [9,10]. For composites with segregated conductive fillers, the conductive path could be drastically changed once deformation happens [11–13], which could lead to declined EMI shielding properties. To solve the above mentioned issue, strategies such as using 3D conductive foams [14,15] and aerogels [16,17] with robust conductive network and carefully designed composition as conductive fillers have been developed to improve the stability of EMI shielding performance. Apart from sophisticated design of compositions, the inner structure also plays a critical role on properties of composites [18–20],

* Corresponding author. School of Mechanical Engineering, Jiangnan University, Wuxi, China.

E-mail address: yuliu@jiangnan.edu.cn (Y. Liu).

<https://doi.org/10.1016/j.compscitech.2021.108652>

Received 8 November 2020; Received in revised form 2 January 2021; Accepted 8 January 2021

Available online 19 January 2021

0266-3538/© 2021 Elsevier Ltd. All rights reserved.

For example, Park et al. introduced highly ordered and periodic porous structure into PDMS elastomers, using an optically patterned 3D nanostructure as a template [18]. The resultant 3D net-shaped PDMS delivered much improved stretchability than its solid counterparts, confirming the feasibility of realizing much higher levels of mechanical properties through controlled structure design. Similarly, extremely stable electrical conductivities were achieved through introducing long-range ordered honeycomb structure into graphene aerogel/PDMS composites [19]. The above findings give us strong implications that desired properties can be obtained through well controlled geometry.

Conventional fabrication techniques of composite materials including machining, casting, and molding produce complex structure through material removal processes, while the ability to control the internal structure is quite limited. 3D printing is an additive manufacturing technique for rapidly producing objects with a wide range of structures while reaching satisfactory geometric accuracy from 3D model data [21]. It has attracted tremendous attention recently to fabricate materials with multifunctional properties and highly ordered structures [22,23]. With exceptional designability and high precision, controllable and stable EMI shielding performance is expected through optimized architecture of the composites.

Herein, we fabricate graphene/polydimethylsiloxane (PDMS) composite with highly ordered lattice structure through 3D printing technique. The resultant composites deliver precisely controlled 3D architecture, with filaments containing uniformly dispersed and effectively reduced graphene oxide (GO) sheets as the construction unit. Exceptional electrical conductivity and mechanical properties are obtained, thanks to the 3D interconnected and robust conductive network. The composites exhibit tunable and stable EMI shielding performance, capable of retaining a high SE of over 25 dB even at a large external tensile strain of 100%, and present negligible SE change after 200 cycles of repeated stretching and releasing.

2. Experimental

2.1. Fabrication of graphene/PDMS inks

Graphene/PDMS inks were fabricated through an *in situ* reduction method. PDMS is chosen as the polymer matrix in this work, due to its excellent printability and stretchability. For the filler, GO dispersion was firstly made by modified Hummers' method based on our previous studies [24,25]. The as-prepared GO slurry was diluted by ethyl acetate to a concentration of 2 mg/mL, followed by ultrasonication for 20 min using a bath sonicator. The resultant GO/ethyl acetate dispersion was mixed with PDMS (SE1700, DOW CORNING)/ethyl acetate solution by magnetic stirring to obtain a uniform GO/PDMS/ethyl acetate solution. Hydroiodic (HI) acid was then added at a HI: GO weight ratio of 10:1 and heated at 90 °C for 12 h to *in situ* reduce the GO sheets. The obtained reduced GO (rGO)/PDMS mixture was vigorously stirred and heat treated at 150 °C until the ethyl acetate was fully evaporated. The resultant uncured and thin-film like rGO/PDMS slurry was immersed in copious amount of DI water for 12 h to completely remove the residual reducing agent, and subsequently dried in a vacuum oven at 60 °C. After cooling down to room temperature, curing agent and inhibitor (3-Butyn-1-ol) were added at a weight ratio of PDMS: curing agent: inhibitor = 100:10:1, and mixed using a planetary mixer (ZYMC-180V, ZYE) at 2000 rpm for 1 min to obtain homogeneous rGO/PDMS inks.

2.2. Fabrication of graphene/PDMS lattice

The as-produced ink is loaded into a 5 cc, luer-lock syringe (Nordson EFD) and centrifuged at 2000 rpm for 3 min followed by 4000 rpm for another 3 min to remove air bubbles. The loaded syringe is then mounted to a specially designed gantry-type 3D printer for the subsequent 3D printing process. The 3D printing system consists of a computer-controlled three-axis moveable platform with the linear

positioning accuracy of $\pm 5 \mu\text{m}$ and a feedback resolution of $1 \mu\text{m}$, a micro-nozzle with an inner diameter of $300 \mu\text{m}$ made of stainless steel, along with a pneumatic dispenser with a pressure resolution of 1 kPa. Highly ordered 3D structures with various distances between two adjacent filaments (d) and filament diameters (w) were fabricated through precisely controlled moves of the X-, Y-, and Z-axes (see Fig. 1a), together with the controlled extrusion of the ink material onto a hydrophobized silicon wafer. The printed samples are cured at 150 °C for 2 h, and then detached from the substrate. The as-produced composite lattices are represented as "graphene/PDMS lattice- d ". For example, the composite with a d value of 0.5 mm are named as graphene/PDMS lattice-0.5. All composites possess 8 layers of filaments with a total thickness of 2.4 mm.

2.3. Characterization

The morphologies of graphene/PDMS ink were examined on a scanning electron microscope (SEM, ZEISS Sigma 500) and confocal laser scanning microscopy (CLSM, LSM 800 for Materials, ZEISS), and the detailed characterization process can be found in Section S1 in the Supplementary Information. The thickness of rGO sheets was characterized using transmission electron microscope (TEM, FEI Tecnai F20). The Raman characterization of PDMS, rGO sheets and graphene/PDMS ink was performed using a Reinshaw MicroRaman/Photoluminescence System. The electrical conductivity of the cured graphene/PDMS ink was measured using four-point probe method (Scientific Equipment & Services). The resistance change of graphene/PDMS composites was recorded using a data logger (34972A, Agilent). A stress-controlled rheometer (DHR-2, TA Instruments) was used to exam the rheological properties of graphene/PDMS ink. The 3D structures of the composite lattices were characterized using an optical microscope (Leica DVM6 A, Leica Microsystems GmbH, Switzerland). The tensile tests were performed on a universal testing machine (ETM102B, WANCE). The EMI shielding properties and complex permittivity was measured by a vector network analyzer (E5063A, Keysight) in X-band frequency range using N1500A software, and the details can be found in Section S2 in the Supplementary Information, similar to our previous work [26].

3. Results and discussion

3.1. Physical properties of graphene/PDMS ink

In this study, direct ink writing (DIW), an extrusion-based 3D printing technique [27–30], is used to construct graphene/PDMS composites into highly ordered and robust lattice structures, as shown in Fig. 1a and b. In order to obtain composites with exceptional functional and mechanical properties, ink materials with exceptional electrical conductivity, along with excellent conformality and printability are highly desired. Herein, an *in situ* reduction method is used to synthesize graphene/PDMS ink, using HI acid as the reduction agent. As illustrated in Fig. 1a, HI acid was added in GO/PDMS mixture to slowly reduce the uniformly dispersed GO sheets inside PDMS/ethyl acetate solution. The as-fabricated ink material was subsequently printed into 3D lattice structure with tailored d and w values, through controlled movement of the three-axis moveable platform and extrusion of the ink material. The resultant composite lattices deliver highly robust and stretchable structure, capable of recovering the original shape even after large tensile deformations, as shown in Fig. 1b.

The composite ink delivers excellent electrical conductivity and low percolation threshold, as shown in Fig. 2a and Section S3 in Supplementary Information, which comes from the effectively reduced GO and uniformly dispersed rGO sheets [31]. Fig. 2b gives the Raman spectra of rGO, PDMS, and rGO/PDMS composites. The D and G bands of rGO sheets can be found at 1344 and 1594 cm^{-1} , respectively, in consistence with the previous studies. The neat PDMS delivers four main peaks at 489, 708, 2906, and 2966 cm^{-1} , corresponding to the symmetric

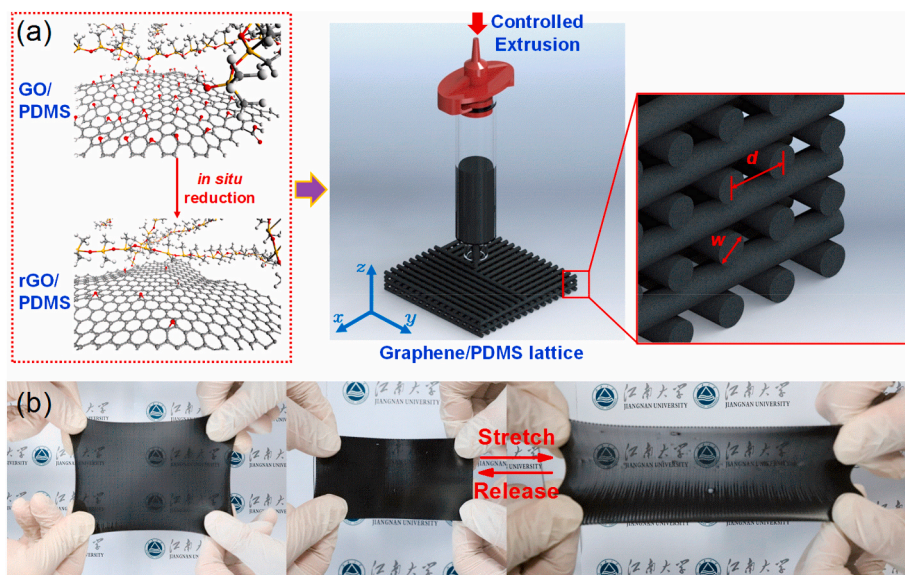


Fig. 1. (a) Fabrication process and (b) digital photographs of graphene/PDMS lattice.

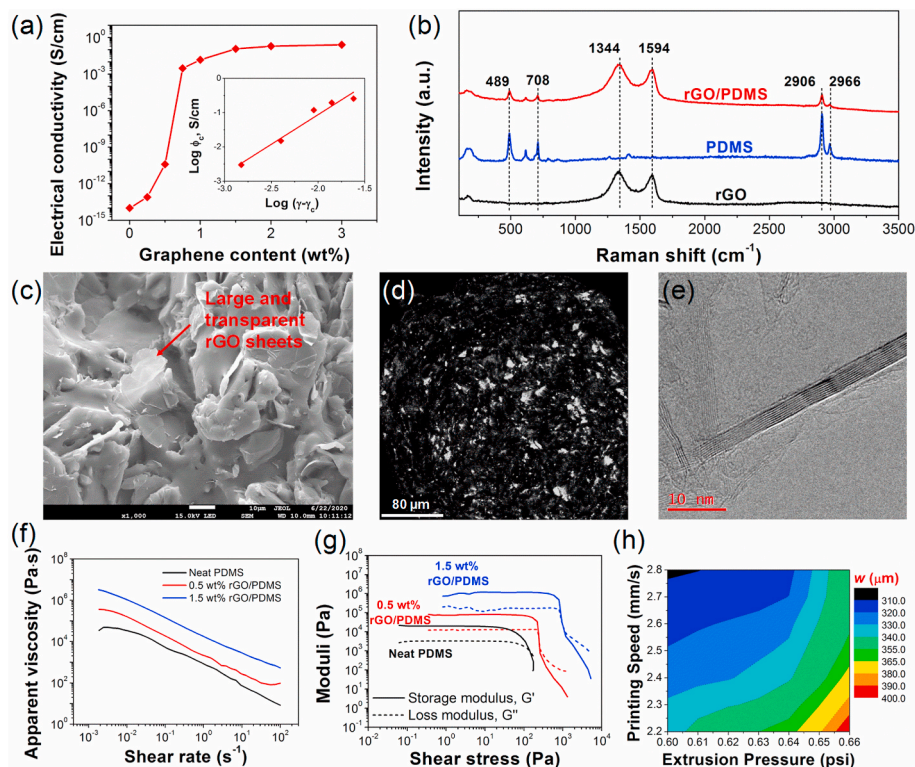


Fig. 2. (a) Electrical conductivity of graphene/PDMS composites, (b) Raman spectra of rGO, PDMS, and rGO/PDMS, (c) SEM and (d) CLSM images of the composites at a graphene content of 1.5 wt%, (e) TEM image of rGO sheets, (f,g) rheological properties of the graphene/PDMS ink, (h) diameter of the printed filaments as a function of printing speed and extrusion pressure.

stretching of Si–O–Si, the symmetric stretching of Si–C, and the asymmetric and symmetric vibrations of CH₃, respectively. The rGO/PDMS ink presents all bands of rGO and PDMS at the same position mentioned above, indicating the uniform dispersion of rGO sheets in the PDMS matrix [32]. The excellent dispersion state of the rGO sheets are further confirmed by the SEM and CLSM images, as shown in Fig. 2c and d. The dispersed rGO sheets contains 4–9 layers of graphene sheets (see the TEM image shown in Fig. 2e), which might come from the slight agglomeration of the rGO during the *in-situ* reduction process. The

effective *in-situ* reduction process lead to the absence of functional groups on the rGO sheets, resulting in limited interactions between graphene and PDMS matrix [33], as the FTIR results shown in Section S4 in Supplementary Information.

The rheological behavior was analyzed to evaluate the printability of the composite ink. As shown in Fig. 2f, both neat PDMS and graphene/PDMS inks deliver shear thinning behavior, and the addition of graphene sheets lead to improved viscosity, arising from the formation of interconnected graphene network inside the PDMS matrix. Similarly,

the storage and loss moduli of the ink increase with the increasing graphene content, as seen in Fig. 2g. Take the composite ink with a graphene content of 1.5 wt% as an example, it exhibits a plateau storage modulus (G') value of $\sim 10^6$ Pa and steeply drops after a yield stress of $\sim 10^3$ Pa, meaning the transition from solid-like to liquid-like behavior. The G' value is about one order of magnitude higher than the loss modulus (G''), confirming the ink is a viscous fluid. The above observation indicates the composite ink is capable of being extruded under strong shear conditions, while it can retain the printed structure without collapsing [34–36]. Take conductivity and printability into consideration, the ink material containing 1.5 wt% graphene was used to fabricate the composite lattice through DIW technique.

3.2. 3D printing and structure of graphene/PDMS lattice

To optimize the printing parameters, the composite ink is extruded using different extrusion pressures and printing speeds. As shown in Fig. 2h, it is found that the diameter of the extruded filaments decrease with the increasing printing speed and decreasing printing pressure, consistent with our previous results [36]. Taking the stability, smoothness, and the production efficiency of the printing process into consideration, a printing speed of 2.6 mm/s, along with an extrusion pressure of 0.62 psi were chosen as the optimized printing parameter, giving a corresponded filament diameter of ~ 320 μm . The optimized filaments are then constructed into highly ordered lattice structures with precisely controlled d values, through designed printing path. As shown in Fig. 3, the as-produced composite lattice delivers long-range ordered and tailored structures, with uniform w values and tunable d values ranging from 400 to 600 μm .

3.3. Mechanical and EMI shielding properties of graphene/PDMS lattice

The highly ordered and precisely controlled structure gives the composite lattices tunable mechanical and EMI shielding properties, as summarized in Table S1 in Supplementary Information. Fig. 4a shows the typical stress-strain curves of graphene/PDMS lattice with different d values. It is seen that the composites are highly stretchable, delivering large elongation at break ranging from over 90%–130%, and the elongation at break increases with the increasing d value. Similar to our previous observation [19,36], such phenomenon is strongly related to the unique 3D lattice structure of the composites. At stretching, the cellular nature of the lattice structure could effectively share the external deformation, giving rise to a lower strain level than the applied external strain. Such assumption is confirmed by the theoretical modeling results. It is clearly seen from Fig. 4h, graphene/PDMS lattice-0.5 deliver low maximum principal strain values of only $\sim 70\%$ at

an external tensile strain of 100%, and the strain level increase with the decreasing d value along all three principal directions (see Fig. 4c). The modeling results indicate the 3D lattice structure is capable of reducing the strain level of the composites, and a larger d value exhibit more remarkable effect, giving rise to a lower strain value and improved stretchability.

Apart from the excellent stretchability and tunable mechanical properties, the tailored structure gives the composites controllable EMI shielding properties. As seen in Fig. 4b, the graphene/PDMS lattices deliver high SE ranging from 25 dB to 45 dB. The SE_T value increases with the decreasing d values, which arises from the denser conductive network for the composites with lower d values. Fig. 4d–f give the SE_R , SE_A , and SE_T of graphene/PDMS lattice-0.5 within X band range. It is seen that the composites present low SE_R values, which comes from the porous surface, leading to limited reflection of the incident EM waves. However, much higher SE_A value of ~ 35 dB are obtained with small fluctuation over the X band range, mainly arising from the highly conductive 3D network effectively absorbing the EM wave. The exceptional EM wave absorption properties give the composite excellent SE_T of ~ 37 dB. The shielding effectiveness continuously increase with the increasing thickness (see Fig. S3 in Supplementary Information), and a highest value of almost 45 dB is achieved at a thickness of 4.8 mm.

To explore the shielding mechanism of graphene/PDMS lattice, the complex permittivity of the composites are measured, as shown in Fig. S4. For conductive polymer composites, the real part of permittivity (ϵ') represents the degree of polarization and the imaginary part (ϵ'') is a measure of dissipated electrical energy [37]. High real and imaginary permittivity are highly desired for EMI shielding materials [38]. It is seen from Fig. S4a that ϵ' increases with the decreasing d value, and gives a highest value of ~ 90 . Such high ϵ' is strongly related to the well dispersed rGO sheets in the composite lattice [39], which results in a large number of micro capacitors and polarization centers. These polarization centers are capable of generating polarization relaxation under alternating EM field and attenuate the field, giving rise to profound energy loss and consequently high ϵ'' value [37], as seen in Fig. S4b. In addition, The well dispersed and conductive graphene network in the composite lattice act as dissipating mobile charge carriers, giving the composites higher EM radiation dissipation via absorption mechanism [38], which validates the observation that absorption contributes much more than reflection in SE_T of the composite lattice.

Besides, alternating current (AC) electrical conductivity of the composites, σ_{AC} , in X-band range is also estimated using the following equation [38,40]:

$$\sigma_{AC}(S/m) = 2\pi f \epsilon_0 \epsilon'' \quad (1)$$

where f is the frequency in Hz, ϵ_0 is the permittivity of free space (8.854×10^{-12} F/m). As shown in Fig. S5, AC conductivity of the composite lattice exhibit high values in the range of 20–50 S/m, much higher than the value (1 S/m) recommended for EMI shielding applications [40]. Therefore, the major EMI shielding mechanisms of graphene/PDMS composite lattice can be ascribed to the following. As illustrated in Fig. 4h, Small amount of EM wave was firstly reflected by the cellular surface. The entered EM wave induces current on the 3D conductive lattice, dissipating most EM energy to thermal energy through polarization relaxation. In addition, the well dispersed and conductive graphene network inside the composites leads to the formation of plentiful insulator-conductor interfaces to induce interfacial polarization, which further dissipate the EM radiation by absorption mechanism. Besides, the residual EM wave could reflect and scatter within the 3D lattice structure many times, giving the composite lattice high EMI SE.

3.4. Shielding stability of graphene/PDMS lattice

Apart from high SE values, stable EMI shielding performance at large

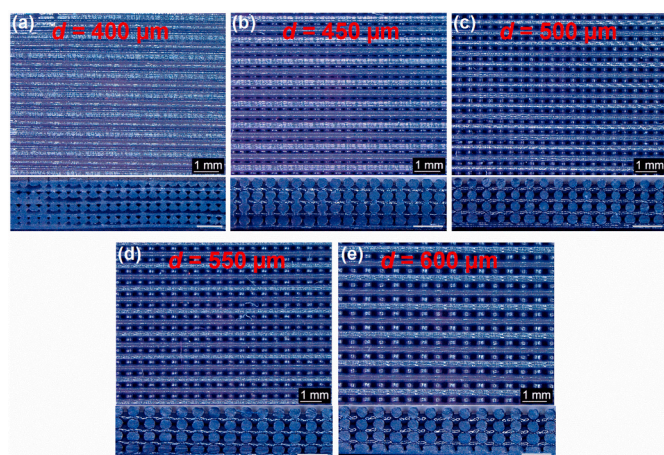


Fig. 3. Optical images of the graphene/PDMS lattice with various d values.

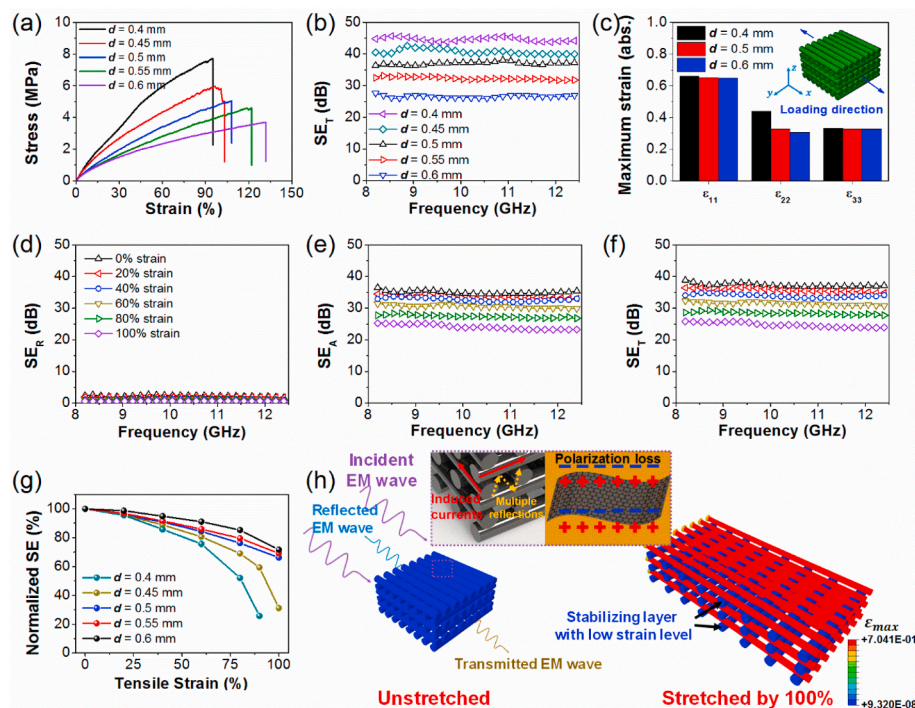


Fig. 4. (a) Stress-strain curves and (b) SE_T of graphene/PDMS lattice with various d values as a function of frequency, (c) Theoretical values of maximum strains along three principal directions for graphene/PDMS lattice with different d values (The inset shows the loading direction), (d) SE_R , (e) SE_A , and (f) SE_T values of graphene/PDMS lattice-0.5 under different tensile strains as a function of frequency, (g) normalized SE_T value of graphene/PDMS lattice with various d values as a functional of tensile strain, (h) schematic illustration of EMI shielding mechanism at large tensile strains for graphene/PDMS lattice.

external deformations is also critical for the application in flexible electronic devices. As shown in Fig. 4d, both SE_R and SE_A decrease with the increasing tensile strain, arising from the changed conductive network and decreased electrical conductivity the composites under external tensile loading [41]. The SE is maintained at ~ 25 dB even under 100% of tensile strain, indicating the exceptional stability of the ordered lattice-structured composites. Fig. 4g summarizes the normalized SE_T of composites with various d values. Similar to the mechanical properties, the shielding stability increase with the increasing d value, resulting from the lower strain level for a larger d at the same external strain. It is also interesting to see that the composites with d values of over 0.5 mm are capable of retaining over 70% of the original SE_T under a large tensile strain of 100%. Such exceptional shielding stability is strongly related to the unique 3D lattice structure of the composites. As demonstrated above, the lattice structure can effectively reduce the strain level on the conductive network of the composites, leading to much smaller resistance change than solid composite film without any inner structural design, as shown in Figs. S6c and d in Supplementary Information. In addition, the filaments perpendicular to the loading directions also play an important role in stabilizing the electrical properties of the composites. As shown in Fig. 4h and Section S9 in Supplementary Information, they exhibit extremely low strain level, which act as stabilizing layer and effectively avoid the drastic resistance change at external strains, thus presenting extremely stable EMI shielding properties.

Fig. 5 gives a comparison of the EMI shielding stability between graphene/PDMS lattice and other stretchable composites made in the open literature. In order to simultaneously achieve excellent stretchability and EMI shielding performance, a commonly used strategy is to incorporate conductive fillers into a stretchable polymer matrix to make composites. However, such composites usually suffer from the instable electrical properties due to the drastically changed conductive network [12,42]. To solve the above issue, researchers have made great efforts on constructing high-quality 3D conductive networks, such as highly conductive MXene [43], graphene aerogel [44], conductive foam [45], and other 3D conductive structures [26,41,46]. These composites are capable of retaining more than 50% of their original SE at a large tensile strain in the range of 25%–200%. In addition, it is interesting to see

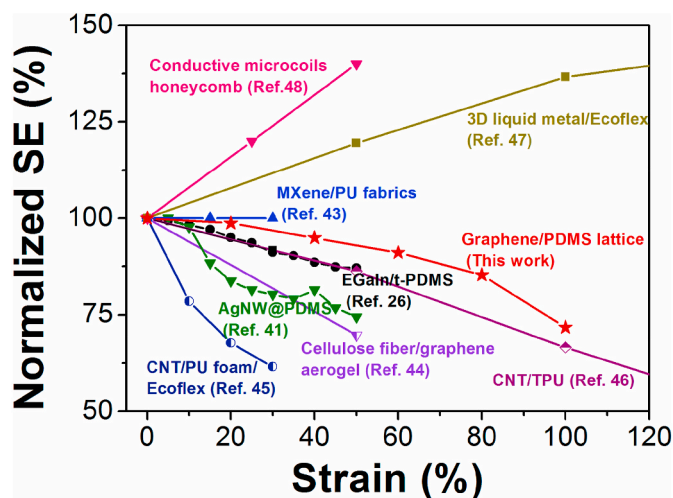


Fig. 5. Comparison of normalized SE between graphene/PDMS lattice and other stretchable EMI shielding composites as a function of tensile strain.

some recent work showing increased SE even under large tensile strains [47,48], where they utilize carefully designed 3D liquid metal structure and highly conductive honeycomb network. In the current work, however, we try to improve the shielding stability through inner structure design of the composites. We construct highly ordered and tailored 3D lattice structure through a facile DIW technique, using well established rGO/PDMS composites as the building block. It is clearly seen from Fig. 5 that the as-produced composite lattice delivers superior stretchability and shielding stability than most conductive EMI shielding composites. The above comparison clearly indicate the advantage of the DIW as a facile and rapid production technique in fabricating composites with stable electrical and mechanical properties. In addition, the composites also exhibit exceptional durability under repeated stretching and releasing. As shown in Fig. S7, the composite lattice remains over 90% of the original SE even after 200 cycles of repeated stretching and releasing, indicating its robust 3D lattice structure and stable conductive

network, which possess exceptional ability to resist external deformations.

4. Conclusions

In summary, we fabricated graphene/PDMS lattices through a facile DIW technique. The resultant composites were highly conductive and stretchable, thanks to the 3D ordered and tailored structure. The 3D interconnected and robust conductive network give the composite lattice exceptional EMI SE and stretchability as high as 45 dB and 130%, respectively. The composite lattice retains 85% and 70% of its original SE under large strains of 90% and 100%, respectively, and delivers negligible performance decline even after 200 cycles of repeated stretching and releasing. Such exceptionally stable and durable performance stems from the unique inner structure of the composite, capable of effectively reducing the strain level on the conductive network and stabilizing the electrical properties at large external strains. The current work provides a facile and rapid production strategy to fabricate multifunctional composites with tailored architecture and properties, through rational design of the inner structure on the basis of targeted application.

Declaration of competing interest

The authors declare that they have no known competing financial interests or personal relationships that could have appeared to influence the work reported in this paper.

Acknowledgments

Financial support from National Natural Science Foundation of China (Grant No. 51905216, 51875253), the Jiangsu Natural Science Foundation (BK20190615), the China Postdoctoral Science Foundation (No. 2018M640451), high-level innovation and entrepreneurship talents introduction program of Jiangsu province of China, the Jiangsu Postdoctoral Science Foundation (No. 2018K012C), the Fundamental Research Funds for the Central Universities (No. JUSR11945), and the Jiangsu Key Laboratory of Advanced Food Manufacturing Equipment and Technology (FMZ201906) is gratefully acknowledged.

Appendix A. Supplementary data

Supplementary data to this article can be found online at <https://doi.org/10.1016/j.compscitech.2021.108652>.

Author contributions

Zhenyu Wang performed writing – original draft, methodology, conceptualization, supervision and funding acquisition

Wenzhen Yang performed methodology and resources

Rui Liu performed methodology and resources

Xingle Zhang performed methodology

Hengyong Nie performed methodology and visualization

Yu Liu performed conceptualization, writing - review & editing, supervision and funding acquisition

References

- [1] G. Wang, X. Liao, J. Yang, W. Tang, Y. Zhang, Q. Jiang, G. Li, Frequency-selective and tunable electromagnetic shielding effectiveness via the sandwich structure of silicone rubber/graphene composite, *Compos. Sci. Technol.* 184 (2019) 107847, <https://doi.org/10.1016/j.compscitech.2019.107847>.
- [2] J. Luo, S. Zhao, H. Zhang, Z. Deng, L. Li, Z. Yu, Flexible, stretchable and electrically conductive MXene/natural rubber nanocomposite films for efficient electromagnetic interference shielding, *Compos. Sci. Technol.* 182 (2019) 107754, <https://doi.org/10.1016/j.compscitech.2019.107754>.
- [3] C. Ge, G. Wang, X. Li, J. Chai, B. Li, G. Wan, G. Zhao, G. Wang, Large cyclic deformability of microcellular TPU/MWCNT composite film with conductive stability, and electromagnetic interference shielding and self-cleaning performance, *Compos. Sci. Technol.* 197 (2020) 108247, <https://doi.org/10.1016/j.compscitech.2020.108247>.
- [4] G. Wang, Q. Yu, Y. Hu, G. Zhao, J. Chen, H. Li, N. Jiang, D. Hu, Y. Xu, Y. Zhu, A. G. Nasibulin, Influence of the filler dimensionality on the electrical, mechanical and electromagnetic shielding properties of isoprene rubber-based flexible conductive composites, *Compos. Commun.* 21 (2020) 100417, <https://doi.org/10.1016/j.coco.2020.100417>.
- [5] Y. Chen, L. Pang, Y. Li, H. Luo, G. Duan, C. Mei, W. Xu, W. Zhou, K. Liu, S. Jiang, Ultra-thin and highly flexible cellulose nanofiber/silver nanowire conductive paper for effective electromagnetic interference shielding, *Compos. Part A.* 135 (2020) 105960, <https://doi.org/10.1016/j.compositesa.2020.105960>.
- [6] D. Feng, P. Liu, Q. Wang, Exploiting the piezoresistivity and EMI shielding of polyetherimide/carbon nanotube foams by tailoring their porous morphology and segregated CNT networks, *Compos. Part A.* 124 (2019) 105463, <https://doi.org/10.1016/j.compositesa.2019.05.031>.
- [7] H. Fang, H. Guo, Y. Hu, Y. Ren, P. Hsu, S. Bai, In-situ grown hollow Fe₃O₄ onto graphene foam nanocomposites with high EMI shielding effectiveness and thermal conductivity, *Compos. Sci. Technol.* 188 (2020) 107975, <https://doi.org/10.1016/j.compscitech.2019.107975>.
- [8] D. Hu, X. Huang, S. Li, P. Jiang, Flexible and durable cellulose/MXene nanocomposite paper for efficient electromagnetic interference shielding, *Compos. Sci. Technol.* 188 (2020) 107995, <https://doi.org/10.1016/j.compscitech.2020.107995>.
- [9] Y. Wu, Z. Wang, X. Liu, X. Shen, Q. Zheng, Q. Xue, J.K. Kim, Ultralight graphene foam/conductive polymer composites for exceptional electromagnetic interference shielding, *ACS Appl. Mater. Interfaces* 9 (2017) 9059–9069, <https://doi.org/10.1021/acsami.7b01017>.
- [10] H. Abbasi, M. Antunes, J.L. Velasco, Recent advances in carbon-based polymer nanocomposites for electromagnetic interference shielding, *Prog. Mater. Sci.* 103 (2019) 319–373, <https://doi.org/10.1016/j.pmatsci.2019.02.003>.
- [11] G. Yang, X. Feng, W. Wang, Q. Ouyang, L. Liu, Z. Wu, Graphene and carbon nanotube-based high-sensitive film sensors for in-situ monitoring out-of-plane shear damage of epoxy composites, *Compos. Part B.* 204 (2021) 108494, <https://doi.org/10.1016/j.compositesb.2020.108494>.
- [12] P. Costa, S. Gonçalves, H. Mora, S.A.C. Carabineiro, J.C. Viana, S. Lanceros-Mendez, Highly sensitive piezoresistive graphene-based stretchable composites for sensing applications, *ACS Appl. Mater. Interfaces* 11 (2019) 46286–46295, <https://doi.org/10.1021/acsami.9b19294>.
- [13] L. Shen, L. Liu, W. Wang, Y. Zhou, In situ self-sensing of delamination initiation and growth in multi-directional laminates using carbon nanotube interleaves, *Compos. Sci. Technol.* 167 (2018) 141–147, <https://doi.org/10.1016/j.compscitech.2018.07.044>.
- [14] X. Sun, X. Liu, X. Shen, Y. Wu, Z. Wang, J.K. Kim, Graphene foam/carbon nanotube/poly(dimethyl siloxane) composites for exceptional microwave shielding, *Compos. Part A.* 85 (2016) 199–206, <https://doi.org/10.1016/j.compositesa.2016.03.009>.
- [15] Z. Chen, C. Xu, C. Ma, W. Ren, H. Cheng, Lightweight and flexible graphene foam composites for high-performance electromagnetic interference shielding, *Adv. Mater.* 25 (2013) 1296–1300, <https://doi.org/10.1002/adma.201204196>.
- [16] Q. Jiang, X. Liao, J. Yang, G. Wang, J. Chen, C. Tian, G. Li, A two-step process for the preparation of thermoplastic polyurethane/graphene aerogel composite foams with multi-stage networks for electromagnetic shielding, *Compos. Commun.* 21 (2020) 100416, <https://doi.org/10.1016/j.coco.2020.100416>.
- [17] S. Zhao, Y. Yan, A. Gao, S. Zhao, J. Cui, G. Zhang, Flexible polydimethylsilane nanocomposites enhanced with a three-dimensional graphene/carbon nanotube bicontinuous framework for high-performance electromagnetic interference shielding, *ACS Appl. Mater. Interfaces* 10 (2018) 26723–26732, <https://doi.org/10.1021/acsami.8b09275>.
- [18] J. Park, S. Wang, M. Li, C. Ahn, J.K. Hyun, D.S. Kim, D.K. Kim, J.A. Rogers, Y. Huang, S. Jeon, Three-dimensional nanonetworks for giant stretchability in dielectrics and conductors, *Nat. Commun.* 3 (2012) 916, <https://doi.org/10.1038/ncomms1929>.
- [19] Z. Wang, X. Liu, X. Shen, N.M. Han, Y. Wu, Q. Zheng, J. Jia, N. Wang, J.-K. Kim, An ultralight graphene honeycomb sandwich for stretchable light-emitting displays, *Adv. Funct. Mater.* 28 (2018) 1707043, <https://doi.org/10.1002/adfm.201707043>.
- [20] Z. Zeng, C. Wang, G. Siqueira, D. Han, A. Huch, S. Abdolhosseinzadeh, J. Heier, F. Nüesch, C. Zhang, G. Nyström, Nanocellulose-MXene biomimetic aerogels with orientation-tunable electromagnetic interference shielding performance, *Adv. Sci.* 7 (2020) 2000979, <https://doi.org/10.1002/advs.202000979>.
- [21] J.R. Raney, B.G. Compton, J. Mueller, T.J. Ober, K. Shea, J.A. Lewis, Rotational 3D printing of damage-tolerant composites with programmable mechanics, *Proc. Natl. Acad. Sci. Unit. States Am.* 115 (2018) 1198–1203, <https://doi.org/10.1073/pnas.1715157115>.
- [22] Y. Yang, X. Li, M. Chu, H. Sun, J. Jin, K. Yu, Q. Wang, Q. Zhou, Y. Chen, Electrically assisted 3D printing of nacre-inspired structures with self-sensing capability, *Sci. Adv.* 5 (2019), eaau9490, <https://doi.org/10.1126/sciadv.aau9490>.
- [23] S.K. Melly, L. Liu, Y. Liu, J. Leng, On 4D printing as a revolutionary fabrication technique for smart structures, *Smart Mater. Struct.* 29 (2020), 083001, <https://doi.org/10.1088/1361-665X/ab9989>.
- [24] Z. Wang, X. Shen, M. Akbari Garakani, X. Lin, Y. Wu, X. Liu, X. Sun, J.K. Kim, Graphene aerogel/epoxy composites with exceptional anisotropic structure and properties, *ACS Appl. Mater. Interfaces* 7 (2015) 5538–5549, <https://doi.org/10.1021/acsami.5b00146>.

- [25] Z. Wang, N.M. Han, Y. Wu, X. Liu, X. Shen, Q. Zheng, J.-K. Kim, Ultrahigh dielectric constant and low loss of highly-aligned graphene aerogel/poly(vinyl alcohol) composites with insulating barriers, *Carbon* 123 (2017) 385–394, <https://doi.org/10.1016/j.carbon.2017.07.079>.
- [26] Z. Wang, J. Ren, R. Liu, X. Sun, D. Huang, W. Xu, J. Jiang, Three dimensional core-shell structured liquid metal/elastomer composite via coaxial direct ink writing for electromagnetic interference shielding, *Compos. Part A* 136 (2020) 105957, <https://doi.org/10.1016/j.compositesa.2020.105957>.
- [27] X. Wan, L. Luo, Y. Liu, J. Leng, Direct ink writing based 4D printing of materials and their applications, *Adv. Sci.* 7 (2020) 2001000, <https://doi.org/10.1002/advs.202001000>.
- [28] J. Zhu, Q. Zhang, T. Yang, Y. Liu, R. Liu, 3D printing of multi-scalable structures via high penetration near-infrared photopolymerization, *Nat. Commun.* 11 (2020) 3462, <https://doi.org/10.1038/s41467-020-17251-z>.
- [29] J.A. Lewis, Direct ink writing of 3D functional materials, *Adv. Funct. Mater.* 16 (2006) 2193–2204, <https://doi.org/10.1002/adfm.200600434>.
- [30] X. Zhu, Y. Chen, Y. Liu, Y. Deng, C. Tang, W. Gao, J. Mei, J. Zhao, T. Liu, J. Yang, Additive manufacturing of elastomeric foam with cell unit design for broadening compressive stress plateau, *Rapid Prototyp. J.* 9 (2017) 1579–1585, <https://doi.org/10.1108/RPJ-09-2017-0172>.
- [31] Z. Wang, X. Shen, N.M. Han, X. Liu, Y. Wu, W. Ye, J.K. Kim, Ultralow electrical percolation in graphene aerogel/epoxy composites, *Chem. Mater.* 28 (2016) 6731–6741, <https://doi.org/10.1021/acs.chemmater.6b03206>.
- [32] Y. Tang, Z. Zhao, H. Hu, Y. Liu, X. Wang, S. Zhou, J. Qiu, Highly stretchable and ultrasensitive strain sensor based on reduced graphene oxide microtubes-elastomer composite, *ACS Appl. Mater. Interfaces* 7 (2015) 27432–27439, <https://doi.org/10.1021/acsami.5b09314>.
- [33] A.N. Parvez, M.H. Rahaman, H.C. Kim, K.K. Ahn, Optimization of triboelectric energy harvesting from falling water droplet onto wrinkled polydimethylsiloxane-reduced graphene oxide nanocomposite surface, *Compos. Part B* 174 (2019) 106923, <https://doi.org/10.1016/j.compositesb.2019.106923>.
- [34] S.J. Talley, B. Branch, C.F. Welch, C.H. Park, J. Watt, L. Kuettner, B. Patterson, D. M. Dattelbaum, K. Lee, Impact of filler composition on mechanical and dynamic response of 3-D printed silicone-based nanocomposite elastomers, *Compos. Sci. Technol.* 198 (2020) 108258, <https://doi.org/10.1016/j.compscitech.2020.108258>.
- [35] Y. Guo, Y. Liu, J. Liu, J. Zhao, H. Zhang, Z. Zhang, Shape memory epoxy composites with high mechanical performance manufactured by multi-material direct ink writing, *Compos. Part A* 135 (2020) 105903, <https://doi.org/10.1016/j.compositesa.2020.105903>.
- [36] Z. Wang, W. Gao, Q. Zhang, K. Zheng, J. Xu, W. Xu, E. Shang, J. Jiang, J. Zhang, Y. Liu, 3D-printed graphene/polydimethylsiloxane composites for stretchable and strain-insensitive temperature sensors, *ACS Appl. Mater. Interfaces* 11 (2018) 1344–1352, <https://doi.org/10.1021/acsami.8b16139>.
- [37] S.K. Marka, B. Sindam, K.C.J. Raju, V.V.S.S. Srikanth, Flexible few-layered graphene/poly vinyl alcohol composite sheets: synthesis, characterization and EMI shielding in X-band through the absorption mechanism, *RSC Adv.* 5 (2015) 36498–36506, <https://doi.org/10.1039/c5ra04038h>.
- [38] M.H. Al-saleh, W.H. Saadeh, U. Sundararaj, EMI shielding effectiveness of carbon based nanostructured polymeric materials : a comparative study, *Carbon* 60 (2013) 146–156, <https://doi.org/10.1016/j.carbon.2013.04.008>.
- [39] A.N. Esfahani, A. Katbab, A. Taeb, L. Simon, M.A. Pope, Correlation between mechanical dissipation and improved X-band electromagnetic shielding capabilities of amine functionalized graphene/thermoplastic polyurethane composites, *Eur. Polym. J.* 95 (2017) 520–538, <https://doi.org/10.1016/j.eurpolymj.2017.08.038>.
- [40] F. Shahzad, S.H. Lee, S.M. Hong, C.M. Koo, Segregated reduced graphene oxide polymer composite as a high performance electromagnetic interference shield, *Res. Chem. Intermed.* 44 (2018) 4707–4719, <https://doi.org/10.1007/s11164-018-3274-7>.
- [41] J. Jung, H. Lee, I. Ha, H. Cho, K.K. Kim, J. Kwon, P. Won, S. Hong, S.H. Ko, Highly stretchable and transparent electromagnetic interference shielding film based on silver nanowire percolation network for wearable electronics applications, *ACS Appl. Mater. Interfaces* 9 (2017) 44609–44616, <https://doi.org/10.1021/acsami.7b14626>.
- [42] S. Kumar, T.K. Gupta, K.M. Varadarajan, Strong, stretchable and ultrasensitive MWCNT/TPU nanocomposites for piezoresistive strain sensing, *Compos. Part B* 177 (2019) 107285, <https://doi.org/10.1016/j.compositesb.2019.107285>.
- [43] W. Yuan, J. Yang, F. Yin, Y. Li, Y. Yuan, Flexible and stretchable MXene/Polyurethane fabrics with delicate wrinkle structure design for effective electromagnetic interference shielding at a dynamic stretching process, *Compos. Commun.* 19 (2020) 90–98, <https://doi.org/10.1016/j.coco.2020.03.003>.
- [44] Y. Wan, P. Zhu, S. Yu, R. Sun, C. Wong, W. Liao, Ultralight, super-elastic and volume-preserving cellulose fiber/graphene aerogel for high-performance electromagnetic interference shielding, *Carbon* 115 (2017) 629–639, <https://doi.org/10.1016/j.carbon.2017.01.054>.
- [45] K. Huang, M. Chen, G. He, X. Hu, W. He, X. Zhou, Y. Huang, Z. Liu, Stretchable microwave absorbing and electromagnetic interference shielding foam with hierarchical buckling induced by solvent swelling, *Carbon* 157 (2020) 466–477, <https://doi.org/10.1016/j.carbon.2019.10.059>.
- [46] D. Feng, D. Xu, Q. Wang, P. Liu, Highly stretchable electromagnetic interference (EMI) shielding segregated polyurethane/carbon nanotube composites fabricated by microwave selective sintering, *J. Mater. Chem. C* 7 (2019) 7938–7946, <https://doi.org/10.1039/c9tc02311a>.
- [47] B. Yao, W. Hong, T. Chen, Z. Han, X. Xu, R. Hu, J. Hao, C. Li, H. Li, S.E. Perini, M. T. Lanagan, S. Zhang, Q. Wang, H. Wang, Highly stretchable polymer composite with strain-enhanced electromagnetic interference shielding effectiveness, *Adv. Mater.* 32 (2020) 1907499, <https://doi.org/10.1002/adma.201907499>.
- [48] C. Liu, J. Cai, P. Dang, X. Li, D. Zhang, Highly stretchable electromagnetic interference shielding materials made with conductive microcoils confined to a honeycomb structure, *ACS Appl. Mater. Interfaces* 12 (2020) 12101–12108, <https://doi.org/10.1021/acsami.0c00034>.